Surface treatment impact on fatigue life at 550 °C of the as-built Inconel 718 manufactured by laser-powder bed fusion

Charles Bianchetti, Maria G. Tsoutsouva, Louise Toualbi, Pascale Kanouté

Surface treatment impact on fatigue life at 550°C of the as-built Inconel 718 manufactured by laser-powder bed fusion

C. Bianchetti[a], M. G. Tsoutsouva[a], L. Toualbi[a], P. Kanouté[a]

[a] *Onera - The French Aerospace Lab, Département Matériaux et Structures, F-92322 Châtillon, France*

Abstract

This article compares the impact of surface modification on fatigue life at 550 °C of the Inconel 718 manufactured by laser-powder bed fusion. The surface conditions are as-built, as-machined, shot-peened, oxidized, and combinaisons of those. Surface roughness, microhardness, and residual stress measurements, as well as fractographic analyses are performed to interpret the fatigue results. Fatigue tests show that as-built samples have higher fatigue lifetime than as-machined samples. Moreover, shot peening increases fatigue lifetime. Finally, an oxidation treatment at 550 °C during 41.6 days does not affect fatigue life.

Keywords: additive manufacturing, laser-powder bed fusion, Inconel 718, fatigue, shot peening, oxidizing, elevated temperature.

1. Introduction

Metal additive manufacturing is a disruptive technology that is likely to replace some traditional manufacturing processes. Among the many available

additive manufacturing processes, the present study focuses on the laser-power bed fusion (L-PBF) process.

Metal additive manufacturing offers numerous advantages including faster and lower-priced production [1] for more complex geometries [2]. The working principle of these processes consists in adding feedstock material layer upon layer until shaping the desire piece. However, this process creates undesirable high surface roughness [3], porosity [4], and tensile residual stresses [5]. These side effects involve that as-built (AB) test pieces have drastic inferior fatigue life in comparison with that of the conventional counterparts [3, 6]. In materials science, fatigue life characterizes the ability of a material submitted to repeatedly loading to withstand without fracturing. Fatigue life is a key parameter in mechanical design, and is currently what disqualify additive manufacturing pieces from being used for critical application. As a consequence, fatigue life of additive manufactured pieces is a hot research topic, with the aim of providing reliable printed structures.

This study focuses on the L-PBF processing of Inconel 718 (IN718) alloy. This nickel-iron based superalloy is widely used, in the form of cast and wrought products, in the aerospace, nuclear and submarine industries for high temperature applications [7]. In recent years, with the increasing maturity of additive manufacturing processes, this alloy has been examined closely in the context of Additive Manufacturing. The microstructure of IN718 is composed of a face-centered cubic matrix, which is strengthened with

precipitates γ" and γ' and fine micrometric precipitates of δ phase located at grain boundaries[4, 8]. Additive manufactured IN718 contains unfavorable compounds regarding mechanical properties such as laves phase and a large amount of acicular delta precipitates decorating the grain boundaries [4, 8]. These detrimental morphology and location of the δ phase are caused by the rapid cooling rate inherent in additive manufacturing process. Moreover, the saturation of δ phases reduces the amount of Nobium available to form the γ" strengthening phase, leading to a potential decrease in the strength of the material. [4, 8]. As a consequence, IN718 pieces additively manufactured are usually heat treated after manufacturing to release potential residual stresses, to reduce the amount of δ phase, and to modify the morphology of these δ precipitates. These post additive manufacturing heat treatments aim also at maximizing the γ' and γ" strengthening precipitates [4, 8].

At room temperature, several authors [3, 9–13, 13, 14] have compared fatigue properties of IN718 pieces additively manufactured with their wrought counterpart. Some reports [10–13] showed that low cycle fatigue (LCF) properties of IN718 pieces additively manufactured in an as-machined (AM) or as-polished (AP) condition were comparable to those of the wrought counterpart. However, the conclusions regarding the comparaison of the fatigue properties in the high cycle fatigue (HCF) regime differ according to the studies. On the one hand, some results showed fatigue properties of additively manufactured IN718 parts in AM or AP conditions comparable

to those of wrought parts [3, 9, 12–14], but on the other hand, some studies showed inferior properties for additively manufactured parts. [9, 12]. The divergent conclusions were likely due to the different heat treatments and surface finishes employed by the authors.

In particular, Lambert [9] compared the fatigue results of IN718 parts produced by additive manufacturing, all subjected to an identical heat treatment but featuring different surface treatments, namely, low stress grinding, bead blasting, and micromachining processes. The results showed that the samples having a low stress grinding surface provided HCF fatigue results comparable to those of a wrought IN718 sheet, while the other surface treatments provided lower fatigue results. Other studies have shown the importance of the surface condition of additively manufactured parts in IN718 on fatigue life [3, 13, 15]. Indeed, these authors have shown experimentally that the fatigue life of the AB condition was significantly lower than that of the AM and AP conditions. For example, Kelley [15] observed that the fatigue lives of AM IN718 samples were 10 and 1000 times higher than those of the AB state in the LCF and HCF regimes, respectively. Such fatigue lifetime difference could partially be attributed to the AB pieces surface roughness, which was about 4 [15] and 10 [3] times higher in average than the AM piece surface roughness. Similar observations regarding the enhancement of fatigue life after machining and polishing were obtained at 427 °C [16] and at 650 °C [16, 17]. However, conclusions regarding those results should be carefully analysed, as the metallurgical state and the materials quality were highly

dependent on the scanning strategies.

High temperature comparison of the fatigue properties of additively manufactured IN718 parts with their wrought counterparts remains rare. Sui *el al.* [18] and Song *et al.* [19] compared the HCF properties of additively manufactured IN718 parts in AP condition with those of their wrought counterparts at 650 °C. Sui *el al.* [18] observed a higher fatigue lifetime for additively manufactured IN718 parts than for wrought parts at low stress amplitudes, but a shorter fatigue life for additively manufactured IN718 parts at high stress amplitudes. However, Song *et al.* [19] observed an opposite trend, with similar fatigue lifetime in HCF for the additively manufacturing and the wrought materials. Sui *el al.* [18] performed a direct aged precipitation treatment on the fabricated samples, while Song *et al.* [19] performed a solid solution annealing prior to double aging, likely resulting in a higher proportion of γ' and γ" precipitates. The two distinct heat treatments employed by the authors could explain the differing conclusions regarding the HCF performance of these additively manufactured samples.

In conclusion, in the HCF regime, fatigue properties of IN718 pieces additively manufactured can be similar to those of the wrought IN718 counterpart under particular conditions. In the LCF regime, fatigue properties at room and high temperatures were similar for additive manufactured and wrought materials. Surface finish and heat treatment appeared to strongly influence the fatigue performance of the IN718 additively manufactured. More specifically, several studies [3, 9, 13, 15–17] suggested that AB pieces should be machined or

polished to improve fatigue performance. Finally, comparaisons of Song *et al.* [19] and Sui *el al.* [18] studies suggested that annealing before aging the AB IN718 improved fatigue performance. Herein, the studied samples were therefore annealing before aging.

Shot peening is a surface treatment commonly used to improve fatigue life [20, 21]. The main purpose of shot peening consists in impacting a surface with high velocity shots to introduce compressive residual stress, hardening, and potential microstructural changes [20–22]. In addition, this process annihilates the pores near the surface that can be introduced during casting or additive manufacturing [23–25]. However, the shot peening treatment modifies the surface roughness, which may result in a decrease of fatigue properties [20, 21].

The effect of shot peening on fatigue performance of test pieces additively manufactured was studied by Wycisk *et al.* [26], Bagherifard *et al.*[27], and Wood *et al.* [28] for Ti-6Al-4V, AlSi10Mg, and 316L materials, respectively. These studies showed that shot peening treatements improved fatigue life of AB test pieces. In particular, Bagherifard *et al.* [27] and Wood *et al.* [28] directly shot peened AB test pieces. These shot peening treatments resulted in a large reduction in surface roughness, with an arithmetic mean value of roughness that was 2 [27] and 4 [28] times less than that of the AB surface. This reduced roughness is likely to be partly responsible for the improved fatigue properties.

In regard to IN718 in additive manufacturing, the impact of shot peening on fatigue life was studied at room temperature by Ardi *et al.* [29]. The authors observed that shot peening with S230 media at an Almen intensity of 18A and 200% coverage increased the fatigue life of HCF when compared to AP samples.

Shot peening is traditionally used as a surface treatment to increase fatigue life, although it increases surface roughness which deteriotes fatigue life. In addition, poor fatigue property of additively manufactured structures is the major hindrance for structural applications. Recent studied [26–29] have shown that shot peening decreased surface roughness of additively manufactured samples. Therefore, shot peening appears as a perfect candidate to increase fatigue property of AB additively manufactured material.
The goal of this paper was to verify that shot peening IN718 AB samples was sufficient to obtain at elevated temperature HCF lifetime values as good as those with an AM surface finish. Since IN718 material is usually used for high temperature application effect of oxidation on fatigue life was also studied besides shot peening. For this purpose, AB and AM samples were shot peened and/or oxidized prior to be fatigue testing.

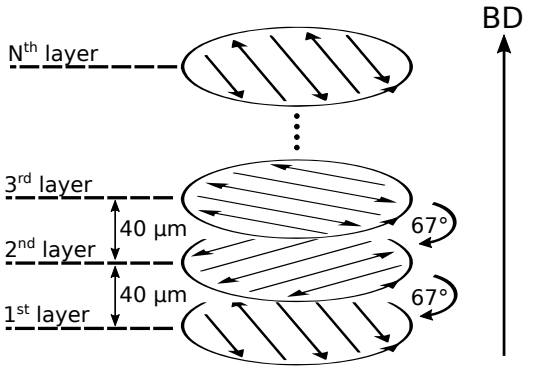

Figure 1: Scanning strategy used to print the fatigue specimens.

2. Material and experimental details

2.1. Material

The studied material was an Inconel 718 nickel superalloy additively manufactured by a L-PBF process. Raw material powder was provided by Praxair with a diameter ranging from 15 to 45 µm. Samples were manufactured using an EOS M280-5 3D printer in a nitrogen inert gas atmosphere. The machine setup is confidential. Specimens were printed following a contour hatch scanning strategy: the outward contours of the studied specimens were first laser printed, then the enclosed surfaces were filled in using a hatch strategy, as shown in Figure 1. The layer thickness was 40 µm and the scanning direction rotated from layer to layer with an angle of 67°, as shown in Figure 1.

2.2. Heat treatments

The residual stresses introduced during the L-PBF process were thermically relaxed to prevent specimens from cracking. Therefore, prior removing from

the support structure, the printed specimens were heat treated at 975 °C during 30 minutes.

The AB microstructure after thermal relaxation contained a high density of δ phases, that limited the potential amount of strengthening γ'' particles precipitation during aging [4]. As a consequence, the printed specimens were heat treated at 1080 °C during 1 hour to dissolve the δ phases, and double aged at 710 °C and at 620 °C both during 8 hours in order to induce the precipitation of the γ' and γ'' phases.

2.3. Microstructure

Figure 2 shows the heat treated microstructure in the plane perpendicular to the building direction (BD), which was the loading direction. Figure 2a presents an inverse pole figure (IPF) map combined with an image quality (IQ) map from electron backscatter diffraction (EBSD) data. This image shows a duplex grain size distribution with finer grains at the surface and within the sample along the scanning direction (SD). These finer grains were the consequence of the high cooling rate induced by the contour hatch scanning strategy. Figure 2b is a scanning electron microscope (SEM) image at low magnification. This figure reveals a high density of porosities within the material, with a large amount of coarse lack of fusions known to have a detriment effect on fatigue life. Finally, a residual amount of the δ phases

located at the grain boundaries was observed at high magnification, as shown in Figure 2c. At first slight, these precipitates were unlikely to have a detrimental effect on fatigue.

2.4. Tensile test

A tensile test was performed in order to provide an idea of the mechanical tensile properties of the printed material. The tensile specimen was loaded in the BD up to a total deformation (ϵ_{tot}) of 2% using a MTS 810 servo-hydraulic test machine. A MTS 652.51C.04 extensometer having a gauge length of 12 mm was used to experimentally measure ϵ_{tot}. The sample was heated at 550 °C using a MTS 653 furnace. The geometry of the tensile specimen was identical to the as-machined fatigue specimen geometry, which is shown in Figure 4c.

The strain rate has been modified during testing to quantitatively evaluate the material's viscosity. For ϵ_{tot} ranging from 0% to 1% and from 1.5% to 2.0%, a strain rate of $10^{-3}\,s^{-1}$ was imposed, while for ϵ_{tot} ranging from 1% to 1.5% the strain rate was set to $10^{-5}\,s^{-1}$.

Table 1 summarizes the tensile properties extracted from the tensile curve shown in Figure 3, and provides the equivalent tensile properties for a conventional IN718 [30]. This table shows that the studied IN718 was similar at high temperature to a conventional counterpart in terms of tensile

Table 1: Tensile properties of the studied material at 550 °C compared to the litterature. E, σ_y, and σ_u are the Young's modulus, the yield strength, and the tensile strength, respectively.

	Temperature [°C]	E [GPa]	σ_y at 0.2% offset [MPa]	σ_u [MPa]
Studied material	550	173	1130	1224
Conventional IN718 [30]	538	172	1068	1275

properties.

Figure 3 presents the tensile test results. This figure shows that viscosity had a minor impact on the material behavior because the stress response was similar at $\epsilon_{tot} = 1\%$ for both strain rates. In addition, a serrated yielding and an abrupt stress response were observed on the tensile curve. This was most likely due to a dynamic strain aging phenomenon, also called Portevin-Le Chatelier effect. This effect has been broadly reported at hight temperature for conventional IN718 [31, 32].

2.5. Surface conditions

Several surface conditions were studied. The baseline conditions were as-built (AB) and as-machined (AM). A number of the AB and AM samples were shot peened (SP) leading to two extra conditions: AB-SP and AM-SP. Similarly, a number of the AB and AM samples were oxidized. The corresponding surface conditions were named AB-Ox and AM-Ox. Finally, a number of the shot peened samples were oxidized. The corresponding surface conditions

Table 2: Studied surface conditions and the corresponding acronyms.

	As-built	As-machined
Baseline	AB	AM
Shot peened	AB-SP	AM-SP
Oxidized	AB-Ox	AM-Ox
Shot peened and oxidized	AB-SP-Ox	AM-SP-Ox

were named AB-SP-Ox and AM-SP-Ox. Table 2 summarizes the eight studied surface conditions along with their acronyms used in the present study. The shot peening and oxidizing conditions are described in Section 2.6.

2.6. Shot peening and oxidizing conditions

Conventional shot peening was performed by an external company, namely, IRT M2P. Samples were shot peened with cut wire 400-700 media, with a nominal Almen intensity of F12A millimeters, and a coverage of 150%. Media were controlled following VDFI 8001 standard [33]. Almen intensities were measured as per SAE J443 standard [34]. Finally coverage were estimated under an optical microscope.

Oxidized samples were heated under constant temperature at 550 °C during 41.6 days (1000 hours) in an air environment. These oxidizing conditions provided a nanometric oxide layer, and therefore did not affect surface roughness.

2.7. Surface roughness measurements

Surface roughness may affect fatigue life results. As a consequence, surface roughness of AB, AB-SP, AM, and AM-SP samples were characterised in the building direction (BD) using a Tribotechnic profilometer. Four profiles were measured per condition at a recording speed of $500\,\mu\mathrm{m}\cdot\mathrm{s}^{-1}$. Arithmetic average roughness (R_a) were extracted from the measured profiles.

2.8. Microhardness measurements

Hardening and residual stress may impact fatigue life results. Microhardness profile provides an indication of hardening and residual stress levels within the material. Thus, in-depth microhardness profiles were measured for the studied surface conditions using a Buehler micromet microhardness tester at a force of 100 g.

2.9. Residual stress measurements

As a complement to the microhardness measurements, surface residual stresses were measured on AM, AB, AB-SP, and SP-Ox samples.

The residual stresses were determined by the x-ray diffraction technique, in which the strain in the crystal lattice was measured, and the residual stress producing the strain was calculated, assuming a linear elastic distortion of the crystal lattice. The measurements were performed in a Panalytical Empyrean X-ray diffractometer equipped with a $\theta - \theta$ goniometer and Cu-Kα ($\lambda =$ 1.5406 Å) as incident radiation, operated at 45 kV and 40 mA. The incident

beam was focused, using 5 mm and 1/4° apertures, on the (420) reflection of the face centered cubic (fcc) Ni-Cr phase ($2\theta = 147.19°$) and the in-plane stress was measured by applying instrumental ω-tilts and performing $\theta - \theta$ scans, in three different directions φ=0°, 45°, 90°.

The analysis was based on the $\sin^2\psi$ method, for which the lattice spacings d were measured at a total of 13 ψ-angles between -50° and 50° (positive and negative ψ-tilts) that correspond to $\sin^2\psi$ values from 0 to 0.6 with steps of 0.1. The stress tensor was calculated by performing a multidirectional stress analysis using the Panalytical's Stress version 2.3 software. Biaxial plane-stress conditions were assumed, involving zero normal stress to the specimen surface (σ_{33}^S). The peak position was found by fitting a Pearson VII profile shape function to the data, and the following intensity corrections were applied on the measured scans: background subtraction, Lorentz-polarization, and K2-stripping. Absorption correction was also applied even though the impact on the intensity was insignificant.

The stresses were determined by a least square fit of the elliptical $\sin^2\psi$ which related the deformation $\epsilon_{\varphi\psi}^{hkl}$, measured by X-ray diffraction, and the components of the stress tensor in the specimen reference frame as follows:

$$\epsilon_{\varphi\psi}^{hkl} = \frac{d_{\varphi\psi}^{hkl} - d_0^{hkl}}{d_0^{hkl}} = \frac{1}{2} S_2^{hkl} (\sigma_\varphi^S - \sigma_{33}^S) \cdot \sin^2\psi + \frac{1}{2} S_2^{hkl} \tau_\varphi^S \sin\psi + \epsilon_{\varphi 0^\circ}^{hkl} \qquad (1)$$

where $\sigma_{\varphi}^{S} = \sigma_{11}^{S} \cdot \cos^2\varphi + \sigma_{12}^{S} \cdot \sin(2\varphi) + \sigma_{22}^{S} \cdot \sin^2\varphi$ is the normal stress, $\tau_{\varphi}^{S} = \sigma_{13}^{S} \cdot \cos\varphi + \sigma_{23}^{S} \cdot \sin\varphi$ the shear stress, $\epsilon_{\varphi 0^\circ}^{hkl} = \frac{1}{2} S_2^{hkl} \sigma_{33}^{S} + S_1^{hkl} (\sigma_{11}^{S} + \sigma_{22}^{S} + \sigma_{33}^{S})$ the strain, σ_{ii}^{S} the normal stress tensor components, and σ_{ij}^{S} the shear stress tensor components.

The slope provided an estimation of residual stress assuming the material X-ray elastic constants $S_1^{420} = -1.48\,\mathrm{TPa}^{-1}$ and $\frac{1}{2} S_2^{420} = 6.61\,\mathrm{TPa}^{-1}$ for the Ni (420), as retrieved from the database of the analysis software, and d_0 the unstressed lattice spacing [35, 36].

2.10. Fatigue tests

The AB samples were directly printed on the built plate in the BD, while the AM samples were extracted from printed cylinders also in the BD, as schematically shown in 4a. The geometry of the AB, AB-SP, and AB-SP-Ox samples is shown on Figure 4b. The geometry of the AM, AM-SP, and AM-SP-Ox samples is shown on Figure 4c. The fatigue tested volume of both geometries were different. In fact, the AB samples had a tested volume 1.8 higher than the AM samples, leading to a potential size effect on the fatigue results. However, the consistency in the crack initiation causes, and the fact that AB samples with higher tested volume had a better fatigue lifetime than AM samples, suggested that the size effect did not impact the present fatigue results.

Axial fatigue tests were performed in the BD under constant stress amplitude

at a stress ratio (R) of 0.1 using a MTS 810 servo-hydraulic test machine at 10 Hz frequency. Samples were heated at 550 °C using a MTS 653 furnace. Three samples were fatigue tested per condition, except for the AM condition where five samples were fatigue tested to approximatively determine the maximum stress required to attain 5×10^4 cycles. This number of cycles were targeted to limit potential fatigue runout after shot peening. Finally, fractured samples were analysed under SEM to determine the crack initiation causes.

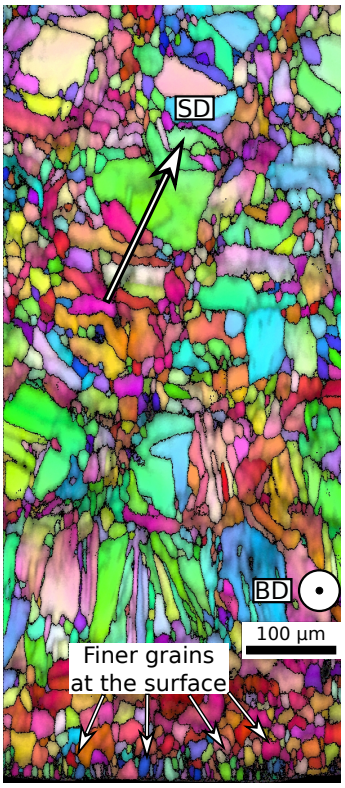

(a) IPF and IQ maps from EBSD

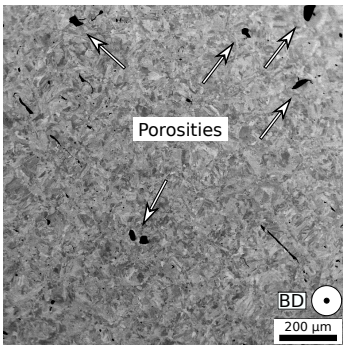

(b) Low magnification

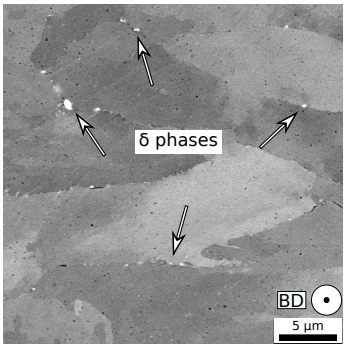

(c) High magnification

Figure 2: Microstructure of the studied material in the plane perpendicular to the BD. (a) Inverse pole figure (IPF) map combined with an image quality (IQ) map from electron backscatter diffraction (EBSD) data. (b) And (c) scanning electron microscope (SEM) images at low and high magnifications, respectively.

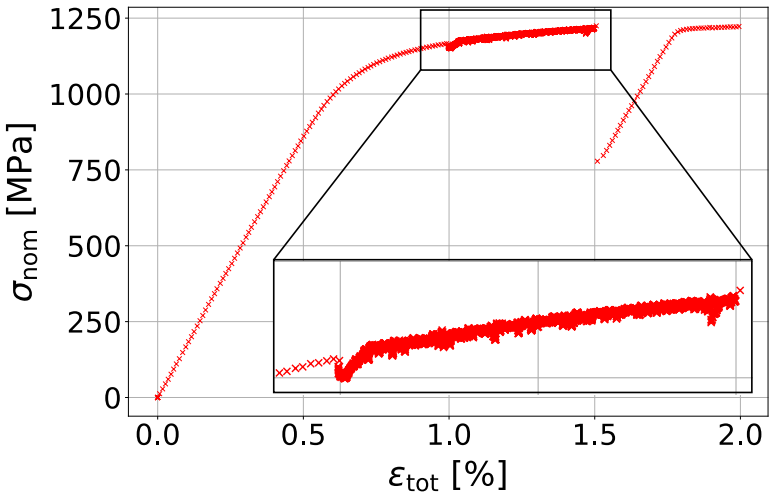

Figure 3: Tensile curve along with a zoom in of the ϵ_{tot} portion tested at a $10^{-5}\,s^{-1}$ strain rate.

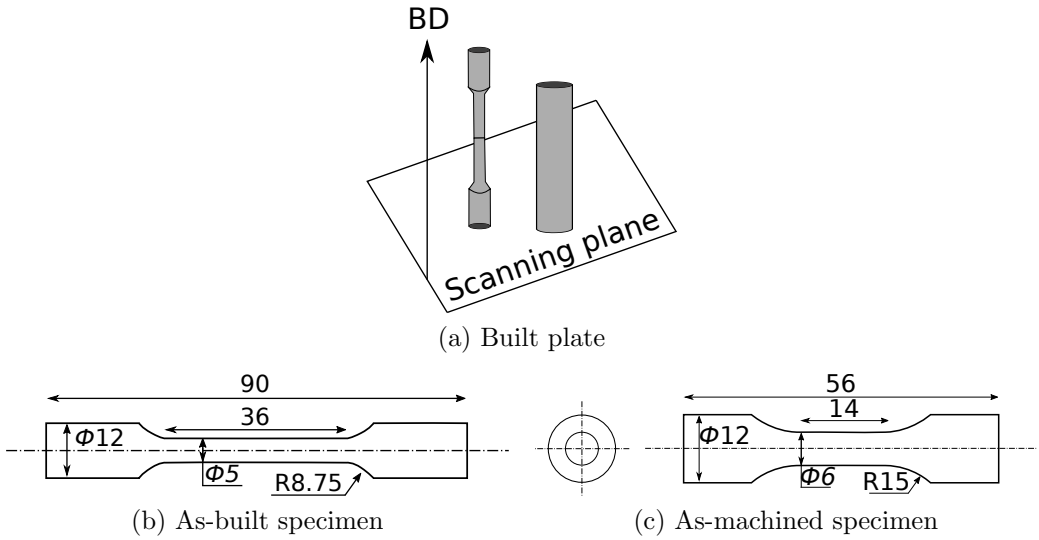

(a) Built plate

(b) As-built specimen

(c) As-machined specimen

Figure 4: Schematic representation of the built plate including one AB sample and one cylinder from which the as-machined specimens were extracted from. (b) And (c) are the geometries of the AB and AM specimens, respectively.

3. Results and discussion

This section describes the fatigue test results. In order to analyse these results, surface roughness, microhardness, and residual stress measurements of the multiple samples subjected to different processing conditions are first presented.

3.1. Surface roughness

Figure 5 shows a histogram of R_a parameter extracted from the measured roughness profiles on AB, AB-SP, AM, and AM-SP samples. Similarly to Kelley *al.* [15], the R_a value of the AB samples was about four times higher in comparison with that of the AM samples. Shot peening decreased surface roughness of AB samples as observed by Bagherifard *et al.*[27] and Wood *et al.* [28]. However, the surface roughness reduction was lower herein with a 1.6 ratio reduction. Finally, shot peened increased surface roughness of AM samples, as commonly observed for machined conventional materials that were shot peened [20, 21].

3.2. Microhardness

Figure 6 provides the measured in-depth microhardness profiles for the AB, AB-SP, AB-Ox, and AB-SP-Ox surface conditions. The horizontal dashed black line at 525 Hv is the AM microhardness baseline. Microhardness of the AB condition was higher over 100 µm subsurface with respect to the AM baseline, with a value of about 550 Hv at the surface. The finer grains

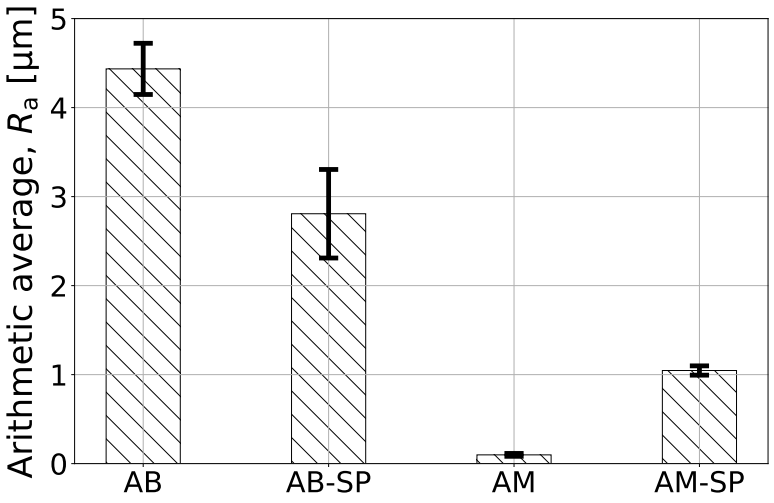

Figure 5: Histogram of the R_a values extracted from surface roughness measurement. The error bars correspond to one standard deviation of uncertainty assuming a normal distribution.

in the near-surface layer induced by the contour scanning strategy, shown on the bottom of Figure 2a, were the cause of this increase as a consequence of the Hall-Petch effect.

Shot peening increased microhardness at 600 Hv over 200 µm below the surface as a result of the surface plastic deformations, which introduced compressive residual stresses and cold-working. Surprisingly, the microhardness values of both oxidation conditions, namely AB-Ox and AB-SP-Ox, upward shifted through the depth. This shift over the entire microhardness profile for the oxidized states suggested a change in the microstructure. The first microstructural characterizations carried out by scanning electron microscopy did not indicate any significant change in the microstructural state between

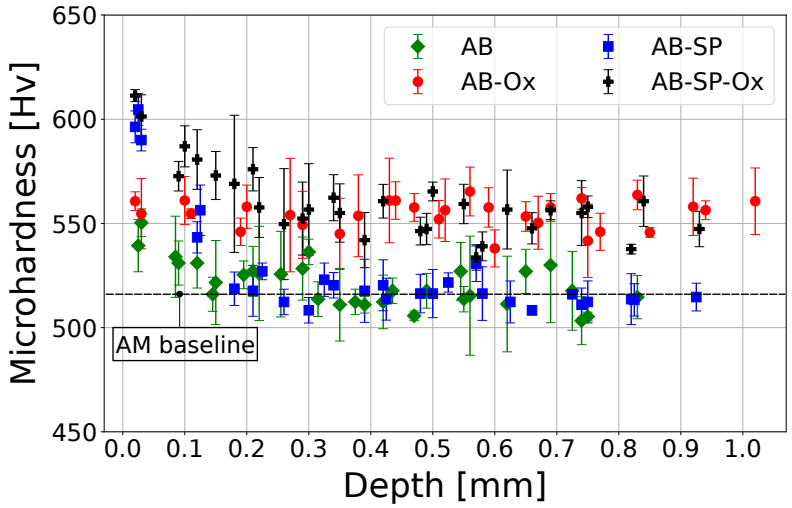

Figure 6: In-depth microhardness profiles of the AB, AB-SP, AB-Ox, and AB-SP-Ox surface conditions. The error bars correspond to one standard deviation of uncertainty assuming a normal distribution.

unoxidized and oxidized samples. These hardness increases were most likely driven by modification at the scale of the nanoprecipitates. Finally, a similar microhardness peak of 600 Hv was measured at the surface of the AB-SP and AB-SP-Ox samples, whereas a decrease in this value was expected after oxidation. Indeed at 540 °C, a thermal relaxation of the residual stresses introduced by shot peening usually occured in conventional IN718 [37]. Consequently, the surface residual stresses were measured on AM, AB, AB-Ox, AB-SP, and AB-SP-Ox in order to quantify the thermal stress relaxation. The corresponding results are presented in the next section.

3.3. Residual stress

Table 3 summarizes the residual stress measured at the surface of the AB, AM, AB-Ox, AB-SP, and AB-SP-Ox samples. The contour hatch scanning technique produced a compressive residual stress on the surface of the printed samples. Indeed, the measured residual stress value of σ_{22} for the AB sample was 75% higher than after machining, where the finer grains at the surface were removed. Shot peening AB samples introduced compressive residual stresses with values of hundreds megapascals. Finally as expected, oxidation induced thermal stress relaxation, with a decrease of 31% and 55% when compared to AB and AB-SP samples, respectively. This relaxation of residual stresses was antagonistic with the increase of the microhardness values after oxidation, as shown in Figure 6. This result suggested a modification of the microstructure during oxidation that would compensate the hardness decrease. Indeed, hardness measurements are complex characterizations, which combines mechanical and microstructural information. As a result, the decrease in hardness due to thermal relaxation of residual stresses were likely compensated by fine precipitation of hardening phase in the oxidized sample.

Finally, the level of thermal stress relaxation was in the same order of magnitude than that observed by Cammett *et al.* [37] for a conventional IN718 at a temparature of 525 °C. However, the authors thermally relaxed their shot peened samples during 10 hours, versus 1000 hours herein. Thus, a higher relaxation rate was expected in the present study. Such a dicreapancy

Table 3: Surface residual stress measurements on AB, AM, AB-Ox, AB-SP, and AB-SP-Ox samples. σ_{11} is the stress tensor component in the building direction, and σ_{22} is the non-zero stress tensor components perpendicular to the building direction, *i.e.*, in the tangential direction of the samples.

Surface condition	σ_{11} [MPa]	σ_{22} [MPa]
AB	-89.1	-112.1
AM	-81.5	-27.3
AB-Ox	-56.6	-82.4
AB-SP	-740.5	-746.3
AB-SP-Ox	-368.5	-298.8

yielded to question whether the particular microstructures of additive manufactured materials changed residual stress relaxation.

3.4. Fatigue results

Figure 7 provides the fatigue results of the tested AM samples. Four stress levels were applied to determine the maximum stress (σ_{max}) corresponding to a fatigue lifetime of 5×10^4 cycles to limit potential fatigue runout set at 1×10^6 cycles after shot peening. Based on these fatigue results, $\sigma_{max} = 650\,\text{MPa}$ was selected for the rest of the study.

Figure 8 presents the fatigue lifetime data for the studied surface conditions. The y-axis indicates the baseline (BS), the oxided (Ox), the shot peened (SP), as well as the shot peened and oxided (SP-Ox) conditions. These conditions are subdivided in AB and AM conditions, which are presented in filled and unfilled symbols, respectively. Figure 8 shows a dual population

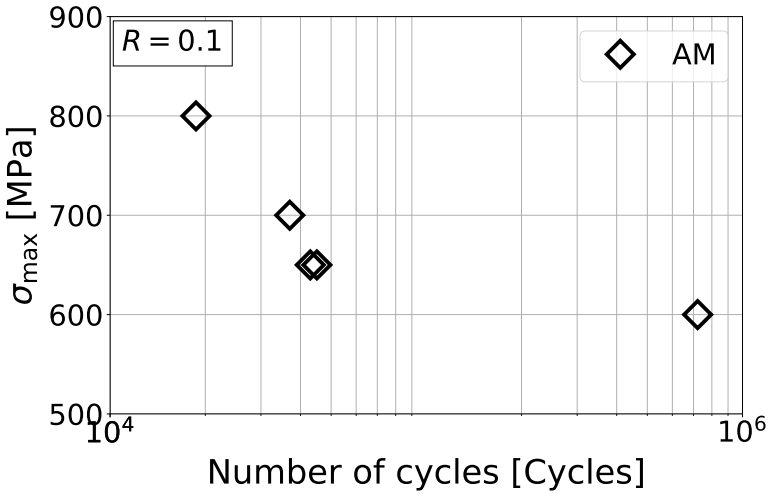

Figure 7: Fatigue lifetime results at 650 MPa for $R = 0.1$ at 550 °C for the AM surface condition.

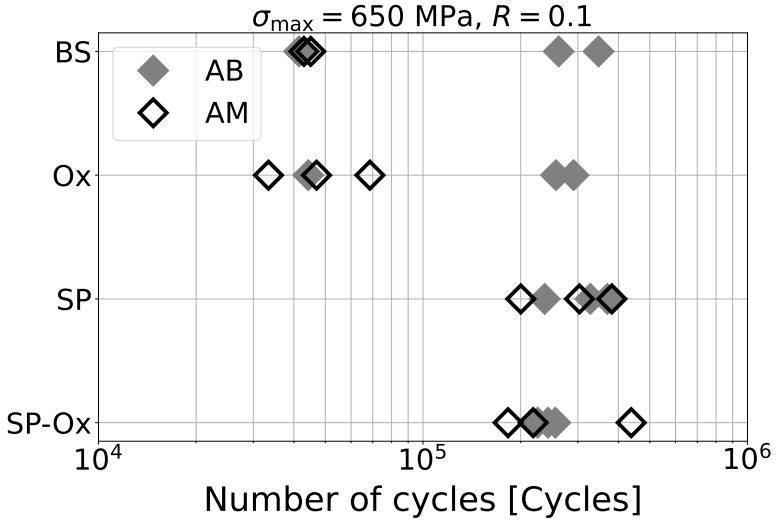

Figure 8: Fatigue lifetime results at 650 MPa for $R = 0.1$ at 550 °C for the studied surface conditions. BS stands for baseline and corresponds to the AB and AM surface conditions

of fractures, approximately at 4×10^4 cycles and 3×10^5 cycles in average. Fractography observations of the tested fatigue samples revealed surface fatigue crack initiations for the samples that fractured around 4×10^4 cycles, and subsurface fatigue crack initiations for the samples that fractured around 3×10^5 cycles. Moreover, fatigue cracks consistently initiated at lack of fusion, except for the AB and AB-Ox samples that fractured around 4×10^4 cycles. Both of these conditions had samples that initiated on a surface discontinuity most likely induced by the L-PBF process. Figure 9 shows a few fracture surfaces that were observed under SEM to support both previous conclusions. Figure 9a presents a surface crack on a lack of fusion that initiated on a AM sample having a fatigue lifetime of 42 959 cycles. Figure 9b shows a surface crack on a surface discontinuity that initiated on a AB sample having a fatigue lifetime of 41 504 cycles. Figure 9c indicates a subsurface crack on a lack of fusion that initiated on a AB sample having a fatigue lifetime of 347 614 cycles. Figure 9d points out a subsurface crack on a lack of fusion that initiated on a AB-SP sample having a fatigue lifetime of 370 012 cycles. Finally, Figure 9d additionally shows an irregular black outline having a flower shape. This outline corresponded to the propagation period, and was observed on most of the fracture surfaces. Close-up view of these flower shapes revealed that porosities were the source of this irregularity in the final crack front.

The present fractographic analysis revealed that porosities drastically undermined the fatigue performance, since porosities were the main source of crack initiations

and reduced the crack growth periods.

Figure 8 also revealed that average fatigue lifetime of AB samples was higher than that of AM samples. As mentioned in the methodology section, the AB samples had a tested volume 1.8 higher than the AM samples, leading to a potential size effect on the fatigue results. However, the size effect would have led to a better fatigue lifetime for the AM samples since the tested volume was smaller.

The fact that AB samples had a better fatigue lifetime than AM samples disagreed with the literature at room temperature [3, 15]. In these articles, the authors listed the higher surface roughness as the prime source of fatigue life reduction for the AB samples. Herein, the surface roughness of AB samples was about four times higher in comparison with that of the AM samples, and thus could not rationalize the observed fatigue life discrepancy. The hypothesis to rationalize the fatigue life discrepancy was the beneficial effect of the contour strategy. First, the contour strategy induced finer grains at the surface of the AB samples, as shown on the bottom of Figure 2a. Those finer grains enhanced the fatigue properties at the surface of the samples [38]. Second, compressive residual stress was 75% higher on AB samples than on AM samples. Finally, the layer built by the contour strategy was likely free of porosities and thus protected the samples from surface crack initiation on lack of fusion. This was consistent with the fractographic analyses described above. Indeed, fatigue cracks of AB and AB-Ox samples never initiated at the

surface on a lack of fusion. The present analysis suggested that the contour strategy had a paramount role in enhancing fatigue performance of the AB samples. In fact, the contour strategy counterbalanced the detrimental roughness effect on fatigue life.

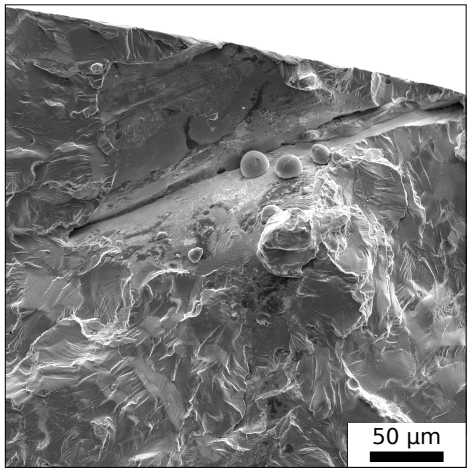

(a) AM: surface crack initiation

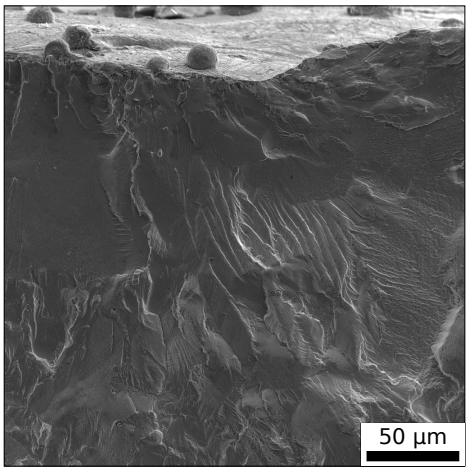

(b) AB: surface crack initiation

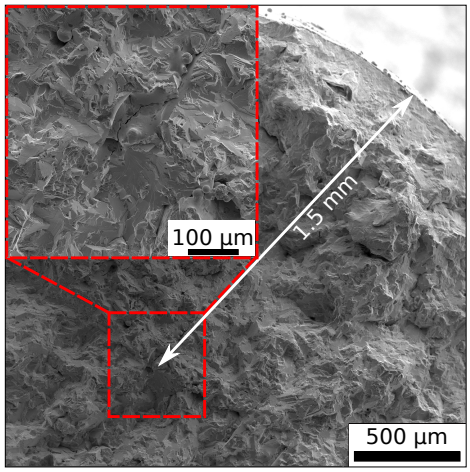

(c) AB: subsurface crack initiation

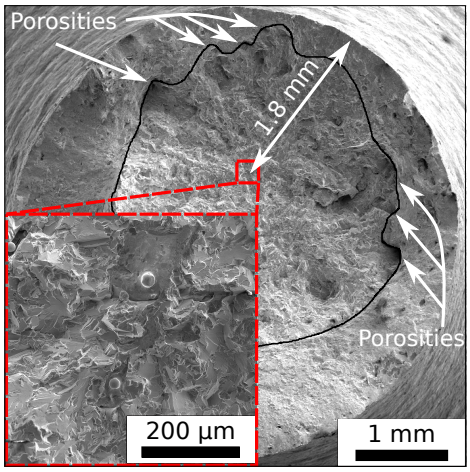

(d) AB-SP: subsurface crack initiation

Figure 9: Fractographic observations of fatigue tested samples having an (a) AM, (b-c) an AB, and (d) an AB-SP surface condition.

As expected, shot peening increased fatigue life in average for AM and AB surface conditions. Fatigue life improvement was 7.5 times higher after shot peening, while Cammett *et al.* [37] observed on a conventional IN718 at 525 °C an improvement of only 2.6 times. Such a large improvement gap was attributed to the inferior fatigue properties of the unpeened samples, due to the large amount of porosities within the printed samples. In fact, Cammett *et al.* [37] observed under an identical stress ratio at 525 °C that the maximum stress reaching 4×10^4 cycles was 1500 MPa for an as-polished sample, which was about 2.3 times higher than that of the printed samples. In addition, Cammett *et al.* [37] observed that the maximum stress reaching 3×10^5 cycles was 1500 MPa for a peened sample, which was about 2.3 times higher than that of the shot peened printed samples. Therefore, even though shot peening improved fatigue life of printed samples, it did not reach fatigue lifetime of shot peened conventional IN718.

In the present study, shot peening prevent surface crack initiation, and thus push the population at 4×10^4 cycles toward 3×10^5 cycles. Shot peening was previously observed to annihilate porosities near the surface [23–25]. However, herein, this annihilation likely had no effect on fatigue life since unpeened specimens had crack initiations either at the surface or subsurface outside the shot peening affected layer. Moreover, based on the present fractographic analysis, surface roughness appeared to play a minor role in the fatigue process. As a consequence, compressive residual stresses were most likely the main shot peening modification that prevented surface crack

initiation.

Finally, it appears that oxidation did not affect the fatigue lifetime even after shot peening where a diminution of fatigue lifetime was expected due to the relaxation of compressive residual stresses. Considering, that oxidized samples had identical surface roughness to the unoxidized counterpart, compressive residual stress most likely led the fatigue process. It appeared that the level of compressive residual stress after oxidation was sufficient to prevent surface crack initiation, and thus hold back fatigue life from decreasing. As a conclusion, oxidizing the samples during 41.6 days at 550 °C dit not impact the fatigue life under the studied stress conditions.

4. Conclusion

Additive manufactured IN718 samples were fatigue tested at 550 °C, with $\sigma_{\max} = 650\,\mathrm{MPa}$, and $R = 0.1$. As-built, as-machined, shot peened, and oxidized surface conditions were studied. The following conclusions were obtained:

- As-built samples had better fatigue lifetime than that of as-machined samples. The contour strategy used to print the samples was considered responsible of this beneficial effect.

- Shot peening strengthened the beneficial effect of the contour strategy on fatigue life.

- Oxidizing the samples during 41.6 days at 550 °C did not impact the fatigue lifetime.

5. Acknowledgments

The authors acknowledge the additive factory hub (AFH) for providing the IN718 samples and for the partial financial support.

References

[1] J. B. Roca, P. Vaishnav, E. R. Fuchs, M. G. Morgan, Policy needed for additive manufacturing, Nature materials 15 (8) (2016) 815–818.

[2] T. Watkins, H. Bilheux, K. An, A. Payzant, R. Dehoff, C. Duty, W. Peter, C. Blue, C. Brice, Neutron characterization, Advanced Materials & Processes (2013) 23.

[3] A. R. Balachandramurthi, J. Moverare, N. Dixit, R. Pederson, Influence of defects and as-built surface roughness on fatigue properties of additively manufactured alloy 718, Materials Science and Engineering: A 735 (2018) 463–474.

[4] E. Hosseini, V. Popovich, A review of mechanical properties of additively manufactured inconel 718, Additive Manufacturing 30 (2019) 100877.

[5] K. S. Sidhu, J. Shi, V. K. Vasudevan, S. R. Mannava, Residual stress enhancement in 3d printed inconel 718 superalloy treated by ultrasonic

nano-crystal surface modification, in: ASME 2017 12th International Manufacturing Science and Engineering Conference collocated with the JSME/ASME 2017 6th International Conference on Materials and Processing, American Society of Mechanical Engineers Digital Collection, 2017.

[6] T. M. Mower, M. J. Long, Mechanical behavior of additive manufactured, powder-bed laser-fused materials, Materials Science and Engineering: A 651 (2016) 198–213.

[7] E. Akca, A. Gürsel, A review on superalloys and in718 nickel-based inconel superalloy, Periodicals of engineering and natural sciences 3 (1).

[8] D. Deng, R. L. Peng, H. Brodin, J. Moverare, Microstructure and mechanical properties of inconel 718 produced by selective laser melting: Sample orientation dependence and effects of post heat treatments, Materials Science and Engineering: A 713 (2018) 294–306.

[9] D. M. Lambert, In718 additive manufacturing properties and influences, in: JANNAF Conference, 2015, pp. 1–14.

[10] E. Sadeghi, P. Karimi, N. Israelsson, J. Shipley, T. Månsson, T. Hansson, Inclusion-induced fatigue crack initiation in powder bed fusion of alloy 718, Additive Manufacturing 36 (2020) 101670.

[11] S. Gribbin, J. Bicknell, L. Jorgensen, I. Tsukrov, M. Knezevic, Low

cycle fatigue behavior of direct metal laser sintered inconel alloy 718, International Journal of Fatigue 93 (2016) 156–167.

[12] A. S. Johnson, S. Shuai, N. Shamsaei, S. M. Thompson, L. Bian, Fatigue behavior and failure mechanisms of direct laser deposited inconel 718, in: Proc. 26th Annu. Int. Solid Free. Fabr. Symp.–An Addit. Manuf. Conf., Austin, 2016, pp. 499–511.

[13] D. B. Witkin, D. Patel, T. V. Albright, G. E. Bean, T. McLouth, Influence of surface conditions and specimen orientation on high cycle fatigue properties of inconel 718 prepared by laser powder bed fusion, International Journal of Fatigue 132 (2020) 105392.

[14] O. Scott-Emuakpor, J. Schwartz, T. George, C. Holycross, C. Cross, J. Slater, Bending fatigue life characterisation of direct metal laser sintering nickel alloy 718, Fatigue & Fracture of Engineering Materials & Structures 38 (9) (2015) 1105–1117.

[15] P. F. Kelley, A. Saigal, J. K. Vlahakis, A. Carter, Tensile and fatigue behavior of direct metal laser sintered (dmls) inconel 718, in: ASME 2015 International Mechanical Engineering Congress and Exposition, American Society of Mechanical Engineers Digital Collection, 2015.

[16] D. M. Lambert, Evaluation of the effect of surface finish on high-cycle fatigue of slm-in718, in: 63rd JANNAF Propulsion meeting, Newport News, VA, United States, 2016.

[17] H. Wan, Y. Luo, B. Zhang, Z. Song, L. Wang, Z. Zhou, C. Li, G. Chen, G. Zhang, Effects of surface roughness and build thickness on fatigue properties of selective laser melted inconel 718 at 650° c, International Journal of Fatigue 137 (2020) 105654.

[18] S. Sui, J. Chen, E. Fan, H. Yang, X. Lin, W. Huang, The influence of laves phases on the high-cycle fatigue behavior of laser additive manufactured inconel 718, Materials Science and Engineering: A 695 (2017) 6–13.

[19] Z. Song, W. Gao, D. Wang, Z. Wu, M. Yan, L. Huang, X. Zhang, Very-high-cycle fatigue behavior of inconel 718 alloy fabricated by selective laser melting at elevated temperature, Materials 14 (4) (2021) 1001.

[20] C. Bianchetti, M. Lévesque, M. Brochu, Probabilistic analysis of the effect of shot peening on the high and low cycle fatigue behaviors of aa 7050-t7451, International Journal of Fatigue 111 (2018) 289–298.

[21] T. Klotz, D. Delbergue, P. Bocher, M. Lévesque, M. Brochu, Surface characteristics and fatigue behavior of shot peened inconel 718, International Journal of Fatigue 110 (2018) 10–21.

[22] J. González, S. Bagherifard, M. Guagliano, I. F. Pariente, Influence of different shot peening treatments on surface state and fatigue behaviour of al 6063 alloy, Engineering Fracture Mechanics 185 (2017) 72–81.

[23] D. Lesyk, V. Dzhemelinskyi, S. Martinez, B. Mordyuk, A. Lamikiz, Surface shot peening post-processing of inconel 718 alloy parts printed by laser powder bed fusion additive manufacturing, Journal of Materials Engineering and Performance 30 (9) (2021) 6982–6995.

[24] D. Lesyk, S. Martinez, B. Mordyuk, V. Dzhemelinskyi, . Lamikiz, G. Prokopenko, Post-processing of the inconel 718 alloy parts fabricated by selective laser melting: Effects of mechanical surface treatments on surface topography, porosity, hardness and residual stress, Surface and Coatings Technology 381 (2020) 125136.

[25] H. Toda, T. Yamaguchi, M. Nakazawa, Y. Aoki, K. Uesugi, Y. Suzuki, M. Kobayashi, Four-dimensional annihilation behaviors of micro pores during surface cold working, Materials transactions 51 (7) (2010) 1288–1295.

[26] E. Wycisk, C. Emmelmann, S. Siddique, F. Walther, High cycle fatigue (hcf) performance of ti-6al-4v alloy processed by selective laser melting, in: Advanced materials research, Vol. 816, Trans Tech Publ, 2013, pp. 134–139.

[27] S. Bagherifard, N. Beretta, S. Monti, M. Riccio, M. Bandini, M. Guagliano, On the fatigue strength enhancement of additive manufactured alsi10mg parts by mechanical and thermal post-processing, Materials & Design 145 (2018) 28–41.

[28] P. Wood, T. Libura, Z. L. Kowalewski, G. Williams, A. Serjouei, Influences of horizontal and vertical build orientations and post-fabrication processes on the fatigue behavior of stainless steel 316l produced by selective laser melting, Materials 12 (24) (2019) 4203.

[29] D. T. Ardi, L. Guowei, N. Maharjan, B. Mutiargo, S. H. Leng, R. Srinivasan, Effects of post-processing route on fatigue performance of laser powder bed fusion inconel 718, Additive Manufacturing 36 (2020) 101442.

[30] L'Alliage 718, une nuance de nickel-chrome durcissable par précipitation, est un super alliage très robuste utilisé à des températures allant jusqu'à 648 °C, NeoNickel (2022).

[31] J. Morris Jr, The influence of grain size on the mechanical properties of steel.

[32] P. Maj, J. Zdunek, M. Gizynski, J. Mizera, K. Kurzydlowski, Statistical analysis of the portevin–le chatelier effect in inconel 718 at high temperature, Materials Science and Engineering: A 619 (2014) 158–164.

[33] Metallisches Strahlmittel Gerundetes Stahldrahtkorn Güteanforderungen, Prüfungen, VDFI 8001 (2009).

[34] J 443 Standard Procedures for Using Standard Shot Peening Almen Test Strip, SAE International (2010).

[35] G. S. Schajer, Practical residual stress measurement methods, John Wiley & Sons, 2013.

[36] B. D. Cullity, Elements of X-ray Diffraction, Addison-Wesley Publishing, 1956.

[37] J. Cammett, P. Prevéy, N. Jayaraman, The effect of shot peening coverage on residual stress, cold work, and fatigue in a nickel-base superalloy, Tech. rep., LAMBDA RESEARCH CINCINNATI OH (2005).

[38] N. E. Dowling, Mechanical behavior of materials: engineering methods for deformation, fracture, and fatigue, pages 445-446, Pearson, 2012.